Visualization of the periodic modulation of Cooper pairing in a cuprate superconductor

Wei Ruan[1], Xintong Li[1], Cheng Hu[2], Zhenqi Hao[1], Haiwei Li[1], Peng Cai[1], Xingjiang Zhou[2,5], Dung-Hai Lee[3,4] and Yayu Wang [1,5]*

In cuprate superconductors, the existence of various intertwined orders associated with spin, charge and Cooper pairs[1,2] is an obstacle in understanding the mechanism of Cooper pairing. The ubiquitous charge order is particularly important[2-7]. Various theories have been proposed to explain the origin of the charge order and its implications for the superconducting phase, including charge stripes[8], electronic nematicity[8,9] and Fermi surface instability[5,10]. A highly appealing physical picture is the 'pair density wave', a spatially periodic modulation of Cooper pairing, which may also induce a charge order[2,11-21]. To elucidate the existence and nature of the pair density wave, we use scanning tunnelling microscopy to investigate a severely underdoped cuprate, in which superconductivity just emerges on top of a pronounced chequerboard charge order. We observe a periodic modulation of both the superconducting coherence peak and gap depth, indicating the existence of a density wave order of Cooper pairing based on the empirical relationship between superconducting coherence and superfluid density[22-27]. The pair density wave has the same spatial periodicity as the charge order, and the amplitudes of the two orders exhibit clear positive correlation. These results shed new light on the origin of and interplay between the charge order and Cooper pairing modulation in the cuprates.

The basic idea of a pair density wave (PDW) dates back to the original proposals in 1964 by Fulde and Ferrell, and independently by Larkin and Ovchinnikov, in which the singlet pairing between the Zeeman-split Fermi surfaces has a finite momentum Q, corresponding to periodic spatial modulations. For cuprate superconductors, several types of PDWs have been proposed to be the origin of the charge order[11-19], including unidirectional[11-13], bidirectional[14] and Ampere pairings[15]. More recently, theories involving the intertwined PDW with d-form factor charge order and superconductivity have been extensively studied[16-19], and it was proposed that both orders share a common wavevector.

Although PDW in the cuprates has been predicted for more than 10 years, direct experimental proof of its existence is still lacking. The main challenge is to probe the spatial distribution of Cooper pairing at the atomic scale. An important recent result is the detection of a PDW state in optimally doped $Bi_2Sr_2CaCu_2O_{8+\delta}$ (Bi-2212) by scanning Josephson tunnelling microscopy (SJTM)[25]. In this technique, a scanning tip is decorated by a nanometre-sized superconducting Bi-2212 flake, and the tunnelling of Cooper pairs between the tip and sample is used to map out the local distribution of Josephson critical current $I_J(r)$. It was found that the superfluid density $\rho_s(r)$

shows a chequerboard pattern indicative of the PDW state, and this shares a common wavevector with the chequerboard charge order. The most probable scenario was proposed to be the coexistence of superconductivity with d-wave symmetry and of charge order with d-symmetry form factor.

If the PDW state is such a pronounced feature, as revealed in the SJTM, one would expect that it should also manifest itself in single-particle tunnelling spectroscopy probed by plain scanning tunnelling microscopy (STM). An obvious strategy is to investigate the spatial distribution of superconducting gap size, but recent theories show that the superconducting gap size may not show spatial periodicity even if there is PDW order[15,16,19-21]. Here we propose that there are two other key characteristics in single-particle tunnelling spectrum that are closely associated with superconductivity. One is the amplitude of the coherence peak near the superconducting gap edge. Although a theoretical understanding of the relationship between the superconducting coherence and superfluid density is still lacking, an empirical positive correlation between these two quantities has been established by experiments with varied doping level and temperature[22-24], Zn substitution for Cu[25,26], and applied magnetic fields[27]. The other is the depth of the superconducting gap, which reflects the depletion (gapping out) of low-energy quasiparticle density of states by Cooper pairing. These two features are directly related to local superconductivity and, as will be shown below, are more sensitive than the gap size to spatial variations of superconductivity.

To detect PDW by using STM, we choose a severely underdoped Bi-2212 with superconducting transition temperature $T_c \approx 10\,K$ (hole density $p \approx 0.06$), in which superconductivity just emerges on doping the parent Mott insulator. At such low doping, the superconducting gap (Δ_0) and pseudogap (Δ_{PS}) are well separated[9,24,28], making it much easier to identify the features associated with superconductivity. Figure 1a displays a large area (600 Å × 600 Å) topographic image acquired on such a Bi-2212 single crystal, where both the atomic structure and supermodulations are clearly resolved. The current map $I(r)$ measured at bias voltage $V = 30\,mV$ in the same field of view and the corresponding Fourier transform are shown in Fig. 1b and c, respectively. The $I(r)$ map measures the spatial distribution of the integrated differential conductance (dI/dV) from the Fermi level to 30 mV. It has a pronounced chequerboard pattern with modulation wavevector magnitude $Q_{CO} = (0.27 \pm 0.04)$ $(2\pi/a_0)$ along the Cu–Cu bond direction, in excellent agreement with the charge order observed in previous STM results on Bi-2212[3-6]. Individual dI/dV maps at several representative energies are

[1]State Key Laboratory of Low Dimensional Quantum Physics, Department of Physics, Tsinghua University, Beijing, P. R. China. [2]Beijing National Laboratory for Condensed Matter Physics, Institute of Physics, Chinese Academy of Sciences, Beijing, P. R. China. [3]Department of Physics, University of California at Berkeley, Berkeley, CA, USA. [4]Materials Sciences Division, Lawrence Berkeley National Laboratory, Berkeley, CA, USA. [5]Innovation Center of Quantum Matter, Beijing, P. R. China. *e-mail: yayuwang@tsinghua.edu.cn
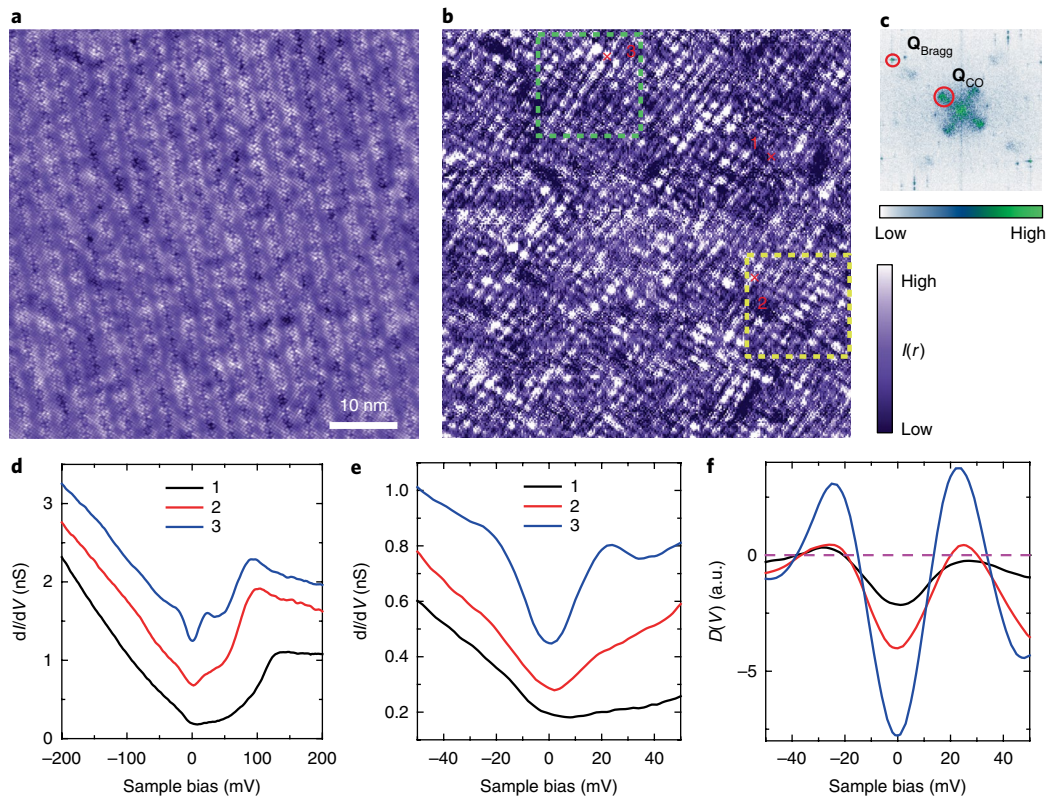
Fig. 1 | Topography, charge order and local electronic structure of underdoped Bi-2212 ($T_c \approx 10$ K). a, Topographic image of a 600 Å square area acquired using bias voltage $V = -300$ mV and tunnelling current $I = 0.5$ nA. **b**, Tunnelling current map $I(r)$ at bias voltage $V = 30$ mV, acquired in the same area as in **a**. The chequerboard charge order is clearly observed. **c**, Fourier transform of the current map, with modulation wavevector magnitude $Q_{CO} = (0.27 \pm 0.04)(2\pi/a_0)$. **d**, Three typical scanning tunnelling spectroscopy curves taken at the spots indicated by red crosses in **b**. Both the pseudogap (approximately 100 mV) and superconducting gap (approximately 20 mV) are resolved. The superconducting gap shows pronounced spatial variations. **e**,The corresponding low-bias spectroscopy of the three curves in **d**. Vertical offset is used for clarity in both **d** and **e**. **f**, Negative of second derivative of the typical spectroscopy curves ($D(V) = -d^3I/dV^3$) with enhanced superconducting coherence peak feature.

displayed in Supplementary Fig. 1, which clearly demonstrate that the chequerboard pattern is a non-dispersive static charge order. To avoid possible set-point effect, all dI/dV curves and mappings are acquired at a set-point bias voltage $V = -300$ mV and tunnelling current $I = 0.5$ nA. These set-up parameters are chosen because the particle–hole asymmetric charge order is much weaker at negative bias[6] and its effect on the set point is negligible (see Supplementary Section C for detailed discussions).

Three representative dI/dV curves are plotted in Fig. 1d, taken at locations marked by the corresponding numbered dots in Fig. 1b. They exhibit strong spatial inhomogeneities, as reported before[29], most probably caused by the random distribution of O defects and Dy dopants. There are two prominent features in these curves: one is the gradual density of states suppression characterized by the peak feature near 100 mV, corresponding to the pseudogap with size $\Delta_{PS} \approx 100$ mV, and the other is the small gap feature between −20 mV and 20 mV, corresponding to the superconducting gap with size $\Delta_0 \approx 20$ mV. For a closer examination of the superconducting features, in Fig. 1e we zoom into the low-bias range of the dI/dV spectra, which reveal pronounced variations of the coherence peaks at the superconducting gap edge (±20 mV). The coherence peaks in the black curve are barely visible, indicating very weak superconductivity. The red curve has clearer features, shown at ±20 mV as two kinks, whereas the blue curve shows very well-defined coherence peaks characteristic of robust superconductivity.

Although it is straightforward to see the variations of the coherence peak amp0litude from the raw dI/dV curves, a more quantitative

analysis helps to reveal its spatial distribution. To selectively characterize the coherence peak, we take the negative of the second derivative $D(V) \equiv -(dI/dV)'' = -d^3I/dV^3$ of each dI/dV curve. Shown in Fig. 1f are the $D(V)$ plots for the three curves in Fig. 1e, which all exhibit peaks near $V = \pm 20$ mV, suggesting that the gap size is almost the same at the three different locations. On the other hand, the peak heights in the D curves are very different, confirming the sensitivity of the second derivative to the strength of superconductivity. By definition, the peak height in the D curve directly reflects the local curvature of the dI/dV spectrum, or the sharpness of the superconducting coherence peak, and is insensitive to the dI/dV value itself. The dI/dV value is affected by extrinsic factors such as local inhomogeneity, which may superimpose different backgrounds onto the low-bias dI/dV features at different locations. Therefore the peak in the D curve serves as a direct and sensitive indicator of the strength of superconducting coherence. The spectroscopic peak feature and its periodic spatial variations cannot be ascribed to the band structure or self-energy effects, mainly because of the particle–hole symmetric behaviour.

Now that the validity of the second derivative representation is justified, we can investigate the spatial distribution of superconducting coherence. Shown in Fig. 2a is a zoomed-in current map in the area indicated by the yellow dashed square in Fig. 1b, and Fig. 2b displays the dI/dV curves acquired along the yellow arrow in Fig. 2a. They already reveal weak but discernible spatial modulations, where the brighter charge puddles have stronger superconducting coherence peaks. The second derivative D signals are calculated numerically
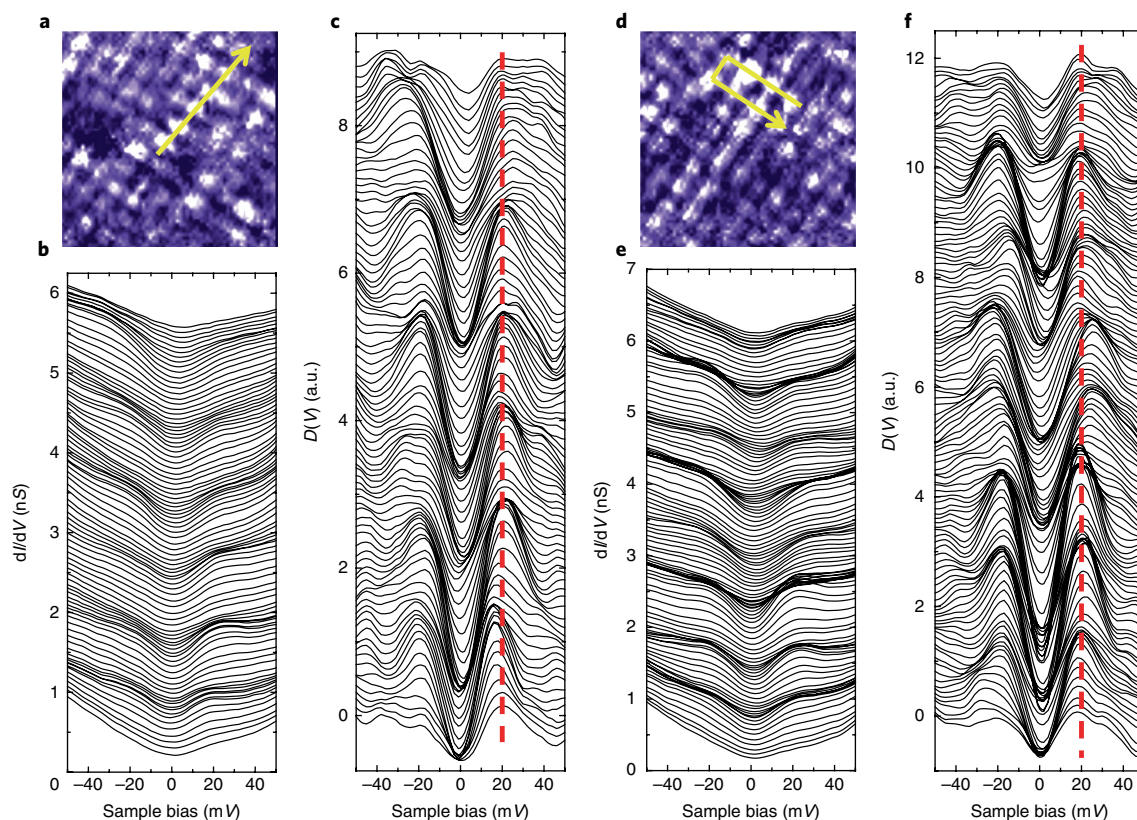
Fig. 2 | Periodic modulations of the superconducting coherence peak feature. a, A close-up of the current map $I(r)$ at bias $V = 30$ mV, in the area as indicated by the yellow dashed square in Fig. 1b. **b**, Low-bias spectroscopy measured along the yellow arrow shown in **a**. **c**, $D(V)$ curves obtained from the scanning tunnelling spectroscopy curves in **b**, where the periodic modulations of the superconducting gap are better visualized by the peaks at ±20 mV. **d**–**f**, The same as **a**–**c**, but for different area, indicated by the green dashed square in Fig. 1b. The spectroscopy and D curves are acquired along the yellow arrow in **d**.

from the dI/dV data and are shown in Fig. 2c. The peak heights at $V = \pm20$ mV in the D curves exhibit periodic spatial patterns in a particle–hole symmetric manner, indicating a periodic modulation of superconducting coherence. The coherence peaks are the strongest at locations where charge accumulates. These observations are confirmed in another area shown in Fig. 2d, corresponding to the green dashed square area in Fig. 1b. The dI/dV curves (Fig. 2e) and the calculated D curves (Fig. 2f) also show periodic spatial modulations that are commensurate with the charge order. The discernible spatial modulation in the raw dI/dV curves and the much enhanced periodic patterns in the D curves are key characteristics of a PDW closely correlated with the charge order.

To directly visualize the PDW order, the dI/dV curves are acquired in a dense grid across the whole area in Fig. 1a. The second derivatives are then calculated for each individual curve at bias $V = 20$ mV, and the $D(r, V = 20$ mV$)$ map is shown in Fig. 3a. This $D(r)$ map clearly exhibits a chequerboard pattern, which suggests a periodic modulation of Cooper-pair density following the empirical positive correlation between the superfluid density and superconducting coherence. Shown in Fig. 3b is the Fourier transform image of the $D(r)$ map, and the PDW wavevector is extracted to be $Q_{PDW} = (0.28 \pm 0.03)(2\pi/a_0)$, which is the same as the charge-order wavevector within the joint error bar. To illustrate the relationship between the two orders, in Fig. 3c we plot the cross correlation of the $D(r)$ and $I(r)$ maps. There is a bright peak located at the centre of the correlation map, indicating that the modulations of charge order and PDW are positively correlated and in phase with each other.

The observation of PDW order from superconducting coherence is further corroborated by the gap depth analysis. As illustrated in
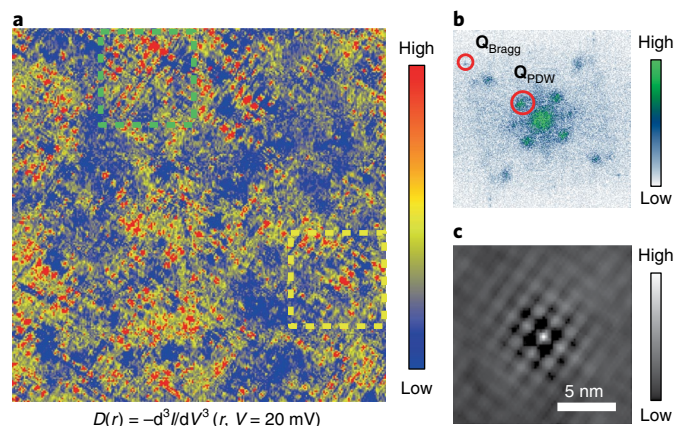
Fig. 3 | Visualization of the pair density wave state by minus second derivative $D(r)$ map. a, Spatial distribution of the superconducting coherence peak feature obtained from the $D(r)$ maps at $V = 20$ mV, which indicates a chequerboard pattern of the Cooper-pair density. **b**, Fourier transform of the D map, with modulation wavevector $Q_{PDW} = (0.28 \pm 0.03)$ $(2\pi/a_0)$. **c**, Cross-correlation map of the $D(r)$ and $I(r)$ (Fig. 1b) maps.

Fig. 4a, the gap depth H is defined as the difference between the coherence peak height and the gap bottom in the dI/dV curve: that is, $H = dI/dV(V = 20$ mV$) - dI/dV(V = 0)$. This quantity directly reflects the amount of low-energy spectral weight that is gapped out by Cooper pairing, and thus it is another indicator of the local
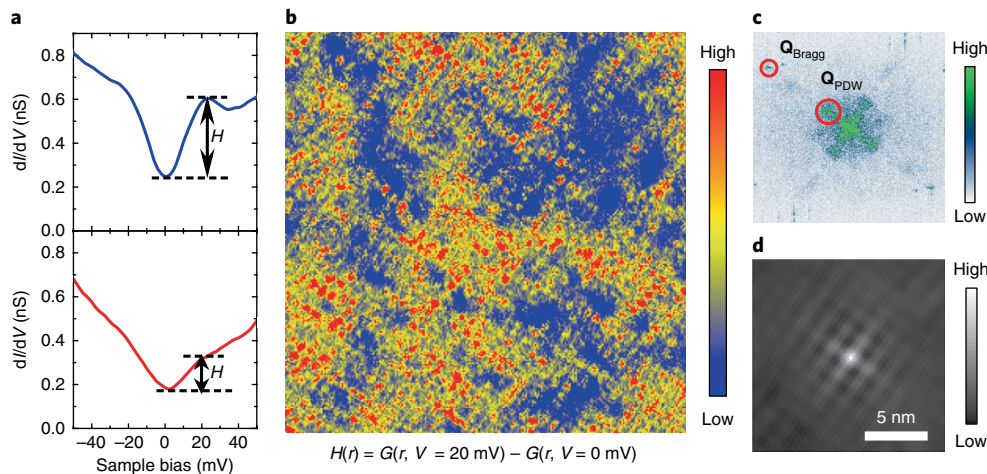
Fig. 4 | Visualization of the PDW state by the gap-depth map $H(r)$. a, Illustration of the gap depth H, which is defined by the superconducting peak height at $V = 20$ mV measured from the zero-bias conductance where the gap bottom sits. **b**, The gap-depth map $H(r)$ defined as the spatially dependent difference of $G \equiv dI/dV$ values at 20 mV and 0 mV, which shows a similar chequerboard pattern, indicating a spatial modulation of the superconducting order parameter $\Delta(r)$. **c**, Fourier transform of the $H(r)$ map, with modulation wavevector $Q_{PDW} = (0.28 \pm 0.04)(2\pi/a_0)$. **d**, Cross-correlation map of the $H(r)$ and $I(r)$ maps.

pair density. Figure 4b depicts the gap-depth map $H(r)$, extracted from the dI/dV curves in the same area, which shows a similar chequerboard pattern to the $D(r)$ map and $I(r)$ map. The modulation wavevector estimated from the Fourier transform (Fig. 4c) is $Q_{PDW} = (0.28 \pm 0.04)(2\pi/a_0)$, consistent with the PDW wavevector extracted from the $D(r)$ map. The cross correlation of $H(r)$ map with the current $I(r)$ map shown in Fig. 4d also displays similar features to those in Fig. 3c, demonstrating a positive correlation between the charge and pair-density modulation strength. The $D(r)$ and $H(r)$ maps defined at $V = -20$ mV for the coherence peak at negative bias are shown in Supplementary Fig. 2. They exhibit the same chequerboard patterns as that for $V = +20$ mV, demonstrating that the PDW order is particle–hole symmetric. Furthermore, we notice that the periodic modulations in the D maps only show up in a narrow bias range around ± 20 mV, whereas the charge order exists for a larger bias range of approximately 40 mV around E_F (see Supplementary Fig. 5). This observation confirms that the observed periodic modulations in the D maps indeed originate from superconductivity rather than the charge order.

The STM experiment and data analysis method described here provide a method of detecting the PDW order from single-particle spectroscopic mapping. Conventional STM data analysis focuses on the dI/dV value at a specific bias voltage, whereas here we scrutinize the overall lineshape of a dI/dV curve, such as the coherence peak sharpness and gap depth, which are indicators of local superconductivity in cuprates given the empirical positive correlation between superconducting coherence and superfluid density. Several important conclusions can be drawn from our results. First, we found that the size of the superconducting gap does not exhibit observable periodic modulations. As shown in Fig. 2c,f, the peak positions of the second derivative plots vary for different locations, but in a rather random manner, presumably owing to local inhomogeneities. In contrast, the superconducting coherence peak and gap depth show clear chequerboard patterns with the same periodicity as the charge order. This observation is consistent with a recent theory showing that, in the presence of intertwined PDW and charge order, the superconducting gap size barely changes whereas the coherence peak and gap depth exhibit a periodic pattern[20,21]. Besides, the charge order mainly gaps out the antinodal Fermi surface whereas superconducting occurs near the nodal direction[24], indicating that the superconducting gap size is unlikely to be affected by the charge order alone. Second, the PDW order is observed in a severely

underdoped Bi-2212 where superconductivity just emerges. Combined with the previous observation of PDW in optimally doped Bi-2212 by SJTM, this indicates that the PDW state seems to exist in a wide range of doping in the cuprate phase diagram. Third, our technique has the advantage of mapping the charge and PDW orders simultaneously, which allow us to show that, at least at this particular doping, the pair density and charge density modulations are positively correlated and in phase with each other. This observation is consistent with theoretical models in which intertwined PDW, d-form factor charge order and d-wave superconductivity coexist[2,13,16–19,30]. Recently, a magnetic-field induced primary PDW order with $8a_0$ periodicity and secondary charge order with $4a_0$ periodicity were reported in nearly optimally doped Bi-2212[31]. These results suggest a different scenario from the $4a_0$ PDW order observed previously by SJTM[25] and that reported here, which will trigger further investigations along this direction.

An issue that deserves further investigation is whether the PDW is a secondary order induced by the charge order, or the other way around. Our previous STM experiment on lightly doped $Bi_2Sr_2CuO_{6+\delta}$ reveals that the charge order emerges from the parent Mott insulator even before the global superconductivity sets in[7]. This suggests that the holes doped into the Mott insulator first form ordered puddles, upon which the PDW order and superconductivity develop. However, it is also possible that owing to strong phase fluctuations at such low doping, the Cooper pairs are strongly localized in space to form a pair crystal, which in return induces a modulated charge distribution. To clarify the exact cause and consequence of these orders, which are critical to the pairing mechanism of cuprates, the narrow regime near the phase boundary when superconductivity just emerges deserves thorough investigation in future STM experiments, using the methodology developed here.

Online content

Any methods, additional references, Nature Research reporting summaries, source data, statements of data availability and associated accession codes are available at https://doi.org/10.1038/s41567-018-0276-9.

References

1. Keimer, B., Kivelson, S. A., Norman, M. R., Uchida, S. & Zaanen, J. From quantum matter to high-temperature superconductivity in copper oxides. *Nature* **518**, 179–186 (2015).
2. Fradkin, E., Kivelson, S. A. & Tranquada, J. M. Colloquium: Theory of intertwined orders in high temperature superconductors. *Rev. Mod. Phys.* **87**, 457–482 (2015).
3. Hoffman, J. E. et al. A four unit cell periodic pattern of quasi-particle states surrounding vortex cores in $Bi_2Sr_2CaCu_2O_{8+\delta}$. *Science* **295**, 466–469 (2002).
4. Hanaguri, T. et al. A 'checkerboard' electronic crystal state in lightly hole-doped $Ca_{2-x}Na_xCuO_2Cl_2$. *Nature* **430**, 1001–1005 (2004).
5. Wise, W. D. et al. Charge-density-wave origin of cuprate checkerboard visualized by scanning tunnelling microscopy. *Nat. Phys.* **4**, 696–699 (2008).
6. da Silva Neto, E. H. et al. Ubiquitous interplay between charge ordering and high-temperature superconductivity in cuprates. *Science* **343**, 393–396 (2014).
7. Cai, P. et al. Visualizing the evolution from the Mott insulator to a charge-ordered insulator in lightly doped cuprates. *Nat. Phys.* **12**, 1047–1051 (2016).
8. Kivelson, S. A. et al. How to detect fluctuating stripes in the high-temperature superconductors. *Rev. Mod. Phys.* **75**, 1201 (2003).
9. Lawler, M. J. et al. Intra-unit-cell electronic nematicity of the high-T_c copper-oxide pseudogap states. *Nature* **466**, 347–351 (2010).
10. Li, J.-X., Wu, C.-Q. & Lee, D.-H. Checkerboard charge density wave and pseudogap of high-T_c cuprate. *Phys. Rev. B* **74**, 184515 (2006).
11. Himeda, A., Kato, T. & Ogata, M. Stripe states with spatially oscillating d-wave superconductivity in the two-dimensional t-t'-J model. *Phys. Rev. Lett.* **88**, 117001 (2002).
12. Corboz, P., Rice, T. M. & Troyer, M. Competing states in the t-J model: uniform d-wave state versus stripe state. *Phys. Rev. Lett.* **113**, 046402 (2014).
13. Berg, E., Fradkin, E., Kivelson, S. A. & Tranquada, J. M. Striped superconductors: how spin, charge and superconducting orders intertwine in the cuprates. *New J. Phys.* **11**, 115004 (2009).
14. Chen, H. D., Vafek, O., Yazdani, A. & Zhang, S. C. Pair density wave in the pseudogap state of high temperature superconductors. *Phys. Rev. Lett.* **93**, 187002 (2004).
15. Lee, P. A. Amperean pairing and the pseudogap phase of cuprate superconductors. *Phys. Rev. X* **4**, 031017 (2014).
16. Seo, K., Chen, H. D. & Hu, J. P. Complementary pair-density-wave and d-wave-checkerboard orderings in high-temperature superconductors. *Phys. Rev. B* **78**, 094510 (2008).
17. Pépin, C., de Carvalho, V. S., Kloss, T., & Montiel, X. Pseudogap, charge order, and pairing density wave at the hot spots in cuprate superconductors. *Phys. Rev. B* **90**, 195207 (2014).
18. Freire, H., de Carvalho, V. S., & Pépin, C. Renormalization group analysis of the pair-density-wave and charge order within the fermionic hot-spot model for cuprate superconductors. *Phys. Rev. B* **92**, 045132 (2015).
19. Wang, Y., Agterberg, D. F. & Chubukov, A. Coexistence of charge-density-wave and pair-density-wave orders in underdoped cuprates. *Phys. Rev. Lett.* **114**, 197001 (2015).
20. Tu, W. L. & Lee, T. K. Genesis of charge orders in high temperature superconductors. *Sci. Rep.* **6**, 18675 (2016).
21. Choubey, P., Tu, W.-L., Lee, T.-K. & Hirschfeld, P. J. Incommensurate charge ordered states in the t-t'-J model. *New J. Phys.* **19**, 013028 (2017).
22. Feng, D. L. et al. Signature of superfluid density in the single-particle excitation spectrum of $Bi_2Sr_2CaCu_2O_{8+\delta}$. *Science* **289**, 277–281 (2000).
23. Gomes, K. K. et al. Visualizing pair formation on the atomic scale in the high-T_c superconductor $Bi_2Sr_2CaCu_2O_{8+\delta}$. *Nature* **447**, 569–572 (2007).
24. Kohsaka, Y. et al. How Cooper pairs vanish approaching the Mott insulator in $Bi_2Sr_2CaCu_2O_{8+\delta}$. *Nature* **454**, 1072–1078 (2008).
25. Hamidian, M. H. et al. Detection of a Cooper-pair density wave in $Bi_2Sr_2CaCu_2O_{8+x}$. *Nature* **532**, 343–347 (2016).
26. Pan, S. H. et al. Imaging the effects of individual zinc impurity atoms on superconductivity in $Bi_2Sr_2CaCu_2O_{8+\delta}$. *Nature* **403**, 746–750 (2000).
27. Pan, S. H. et al. STM studies of the electronic structure of vortex cores in $Bi_2Sr_2CaCu_2O_{8+\delta}$. *Phys. Rev. Lett.* **85**, 1536–1539 (2000).
28. He, Y. et al. Fermi surface and pseudogap evolution in a cuprate superconductor. *Science* **344**, 608–611 (2014).
29. Pan, S. H. et al. Microscopic electronic inhomogeneity in the high-T_c superconductor $Bi_2Sr_2CaCu_2O_{8+x}$. *Nature* **413**, 282–285 (2001).
30. Chakraborty, D., Morice, C. & Pépin, C. Phase diagram of the underdoped cuprates at high magnetic field. *Phys. Rev. B* **97**, 214501 (2018).
31. Edkins, S. D. et al. Magnetic-field induced pair density wave state in the cuprate vortex halo. Preprint at https://arxiv.org/abs/1802.04673 (2018).

Author contributions

W.R. and Y.W. proposed and designed the research. W.R., X.L., Z.H., H.L. and P.C. carried out the STM experiments. W.R. analysed the data with the help from Z.H. and H.L. C.H. and X.Z. provided the Bi-2212 single crystals. D.-H.L. provided theoretical analysis. Y.W. supervised STM experiments and coordinated the collaborations. Y.W. prepared the manuscript with comments from all authors.

Competing interests

The authors declare no competing interests.

Additional information

Supplementary information is available for this paper at https://doi.org/10.1038/s41567-018-0276-8.

Reprints and permissions information is available at www.nature.com/reprints.

Correspondence and requests for materials should be addressed to Y.W.

Publisher's note: Springer Nature remains neutral with regard to jurisdictional claims in published maps and institutional affiliations.

Methods

High-quality Dy doped Bi-2212 single crystals are grown by the floating zone method and are then annealed in vacuum to reach the severely underdoped regime with T_c around 10 K. The STM experiments are performed using a low-temperature ultrahigh-vacuum STM system (CreaTec). For STM experiments, a single crystal is cleaved in ultrahigh vacuum with pressure better than 10^{-10} mbar at $T \approx 77$ K and then immediately transferred to the STM stage sitting at 5 K. Topographic images are scanned using a electrochemically etched tungsten tip which is heated by e-beam and calibrated on an atomically clean Au (111) surface, as described in a previous report[32]. The dI/dV spectra are acquired using standard lock-in technique with reference signal frequency $f = 423$ Hz. The dI/dV spectra and mappings are all measured at tunnelling current $I = 0.5$ nA and bias voltage $V = -300$ mV to avoid set-point effects. The numerical derivative is performed with the Savitzky–Golay method, in which the experimental data are fitted by a second-order polynomial, and the second derivative is obtained from the fitted polynomial.

Data availability

All raw and derived data used to support the findings of this work are available from the authors on request.

References

32. Ye, C. et al. Visualizing the atomic-scale electronic structure of the Ca$_2$CuO$_2$Cl$_2$ Mott insulator. *Nat. Commun.* **4**, 1365 (2013).